Available online at www.sciencedirect.com
ScienceDirect
Journal of Nuclear Materials 361 (2007) 306–312
journal of nuclear materials
www.elsevier.com/locate/jnucmat

An in situ study of the martensitic transformation in shape memory alloys using photoemission electron microscopy

M. Cai [a], S.C. Langford [a], J.T. Dickinson [a,*], Gang Xiong [b], T.C. Droubay [b], A.G. Joly [b], K.M. Beck [b], W.P. Hess [b]

[a] *Department of Physics and Astronomy, Washington State University, Pullman, WA 99164-2814, USA*
[b] *Pacific Northwest National Laboratory, P.O. Box 999, Richland, WA 99352, USA*

Abstract

Thermally-induced martensitic phase transformations in polycrystalline CuZnAl and thin-film NiTiCu shape memory alloys were probed using photoemission electron microscopy (PEEM). Ultra-violet photoelectron spectroscopy shows a reversible change in the apparent work function during transformation, presumably due to the contrasting surface electronic structures of the martensite and austenite phases. In situ PEEM images provide information on the spatial distribution of these phases and the evolution of the surface microstructure during transformation. PEEM offers considerable potential for improving our understanding of martensitic transformations in shape memory alloys in real time.

1. Introduction

Shape memory alloys (SMA) are advanced intelligent materials, whose properties can be programmed to perform specific actions. These alloys exhibit reversible shape changes that can be controlled by the applied stress and/or temperature. This unique property is associated with a solid state martensitic phase transformation [1]. Shape memory alloys are finding important applications in medicine and in microelectromechanical systems [2,3]. More recently, SMA thin films are being investigated for applications in microsensors and microactuators [4,5]. Phase transformations in SMA thin films are often accompanied by significant changes in mechanical, physical, chemical, electrical and optical properties, including yield stress, elastic modulus, damping modulus, hardness, electrical resistivity, thermal conductivity, thermal expansion, and surface roughness [2,6,7].

Martensitic transformations are first order, diffusionless processes involving a shear deformation along the invariant plane (or habit plane). A Bain model (expansion by 12% along two axes with contraction by 20% along the third, normal axis) is usually used to describe the change in structure [8–11]. Specifically, the lattice structure changes associated with the martensitic transformations in CuZnAl (from DO_3 to 18R) and NiTi (from DO_3 to B19)

* Corresponding author. Tel.: +1 509 335 4914; fax: +1 509 335 7816.
E-mail address: jtd@wsu.edu (J.T. Dickinson).

0022-3115/$ - see front matter © 2006 Elsevier B.V. All rights reserved.
doi:10.1016/j.jnucmat.2006.12.008

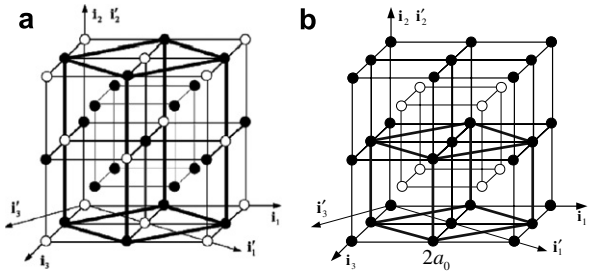

Fig. 1. Lattice configuration of martensite (dark heavy lines) and austenite (light thin lines) for (a) a Cu-based alloy: 18R martensite and DO_3 austenite; and (b) a NiTi alloy: B19 martensite and DO_3 austenite.

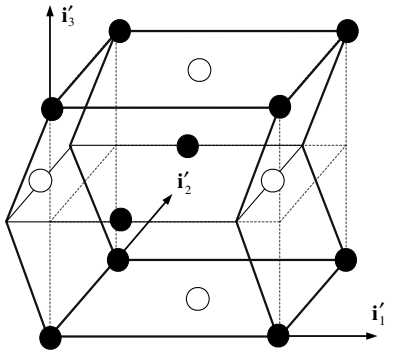

Fig. 2. Atomic displacements associated with a martensitic transformation showing both the Bain and shuffle deformations. The atoms in the center (with open circles) shuffle to the left from the initial position as indicated by the dashed lines.

are illustrated Figs. 1 and 2. These transitions involve a Bain deformation, shown in Fig. 1, and a shuffle deformation, shown in Fig. 2. The shuffle deformation involves an atomic displacement along the i_1' direction in Fig. 2 and does not contribute to the macroscopic change in shape. Austenite is usually the stable phase at high-temperatures. During cooling, cubic austenite changes into monoclinic martensite, sometimes via an intermediate rhombohedral phase (R-phase) in NiTi alloys [12].

The transition from austenite to martensite is typically exothermic. Currently, differential scanning calorimetry (DSC) is a standard technique for determining the temperature-behavior of phase changes during cooling and heating [13]. More recently, modulated differential scanning calorimetry (MDSC) has been developed. MDSC can distinguish reversible and irreversible heat-flow during heating and cooling [14], and thus provides more information than conventional DSC. X-ray diffraction [15,16] and in situ neutron diffraction [17] are also powerful tools for the study of stress- and thermally-induced martensitic transformations; but the acquisition of high-quality data is complicated by the associated crystallographic evolution and residual strain. None of these techniques probe microstructure changes and kinetics simultaneously. In this work, we describe a new experimental technique for nondestructive characterization of structural transitions in SMAs.

Instrumentation for photoemission electron microscopy (PEEM) has recently become commercially available, with lateral resolutions approaching 10 nm [18,19]. The emission of low-energy photoelectrons is extremely sensitive to a variety of surface properties, in particular, the work function. The work function depends on surface chemical composition, crystal orientation, surface dipole, and phase [20–22]. The sensitivity of the work function to surface composition makes PEEM particularly useful for studying surface adsorption, desorption, and surface chemical reactions [23–25]. In this work, we apply photoemission electron microscopy to study the thermally-induced martensitic transformations in CuZnAl- and NiTi-based SMAs. This technique takes advantages of the imaging ability of PEEM and as well as its sensitivity to the apparent work function difference between the austenite and martensite phases to characterize these transformations in situ and in real-time.

2. Experiment

The CuZnAl alloy in this work has a nominal composition of Cu–20.68 wt% Zn–5.8% Al–0.02% Ce–0.02% V, and a thickness of 1.0 mm. The sheet was heat treated at 760 °C for 8 min and quenched in water at 95 °C. The alloy was kept in 95 °C water for 30 min, then cooled to room temperature in the water bath. The lateral grain size is about 1.5 mm. DSC measurements on this material after heat-treatment are shown in Fig. 3. The sample was mechanically polished, ultrasonically cleaned in acetone for 20 min, and then mounted in the ultra-high vacuum PEEM chamber.

The NiTiCu thin film was deposited onto a Si(1 0 0) wafer by magnetron sputtering a NiTi target (50/50 atom percent, 400 W AC power) and a pure Cu target (3-in. diameter, 2 W DC power). The substrate was held at 450 °C and rotated during deposition. The deposition rate was 14.6 nm/min,

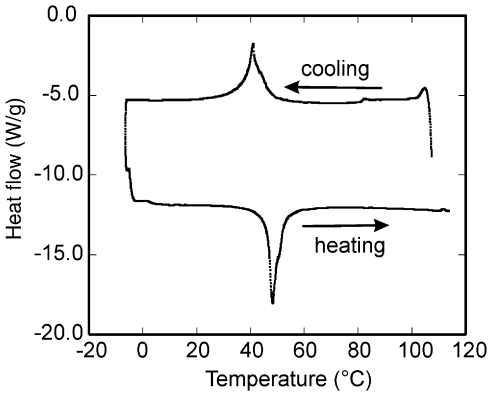

Fig. 3. Differential scanning calorimetric plot for CuZnAl during a thermal cycle.

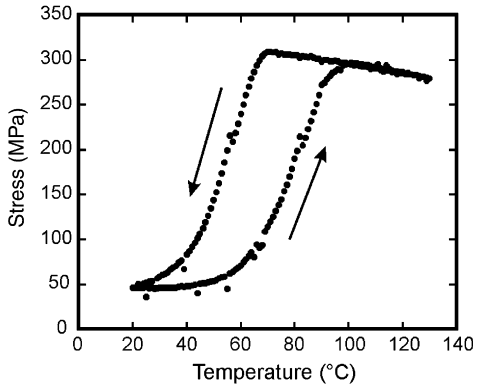

Fig. 4. Film stress versus temperature plot derived from curvature measurements after post-annealing. The hysteresis of the curve during heating/cooling reflects the shape memory effect.

yielding a final film thickness of 3.5 ± 0.3 μm. Samples were post-annealed in vacuum (1×10^{-6} Torr) at 650 °C for 1 h. Film stress measurements, acquired with a Tencor FLX-2908 Thin Film Stress Measurement System during heating at 1 °C/min and air cooling (average cooling rate about 1 °C/min), are shown in Fig. 4.

The work functions of both samples were determined by ultraviolet photoelectron spectroscopy (UPS), using a GammaData/Scienta SES 200 Photoelectron Spectrometer with a He I UV lamp. Photoemission electron microscope images were acquired with an Elmitec PEEM III instrument. Ultraviolet light, with photon energies up to 5 eV, was provided by an Oriel 100 W DC mercury lamp. Prior to imaging, the samples were sputtered in argon (4×10^{-4} Pa) for 15 min (12 mA, 1500 V). Real-time images during heating and cooling were recorded as movie frames.

3. Results and discussion

3.1. Microstructure changes during phase transformation

Fig. 5 shows PEEM images of a polished CuZnAl SMA before and after the phase transformation during heating. The spear-like structures in Fig. 5(a) are martensite plates within a single martensite grain. Because the sample was polished at room temperature, while the sample was in the martensite phase, the transformation to austenite roughens the surface. Polishing scratches on the low-temperature phase (marked by the arrow in Fig. 5(a)) are obscured by this roughness on the high-temperature phase in Fig. 5(b). Although the internal plate structure of the martensite is destroyed by the transformation to austenite, the associated spear-like surface features are simply displaced. These changes are completely reversible upon cooling. During cooling, the formation of martensitic variants within grains (to form martensie plates) is readily observed.

The displacement of the spear-like microstructure during the phase transformation is expected due to the shear-dominant feature of martensitic transformation. We attribute the disappearance of the scratch lines on high-temperature phase to a significant increase in surface roughness: the vertical relief associated with the spear-like structures is significantly greater on the austenite than on the martensite, perhaps due to lattice sliding. This increased surface relief is responsible for the thicker shadows in Fig. 5(b) relative to Fig. 5(a). Fig. 6 shows root-mean-square roughness measurements derived from profilemetry measurements during three thermal cycles. The RMS roughness of the austenite phase is at least double that of the martensite phase. Similar surface relief phenomena have been observed on NiTi and Fe–Mn–Si SMA surfaces [26,27].

PEEM images of the NiTiCu SMA film at 25 °C (martensite phase) and at 100 °C (austenite phase) are shown in Fig. 7. The most prominent difference between the images is the presence of wrinkle-like features on the surface of the low-temperature surface of Fig. 7(a), and their absence on the high-temperature surface of Fig. 7(b). The transition between the wrinkled and smooth states is remarkably sharp. Sequences of PEEM images indicate that the wrinkles disappear at 73.1 °C during heating and reappear at 52.4 °C during cooling. The

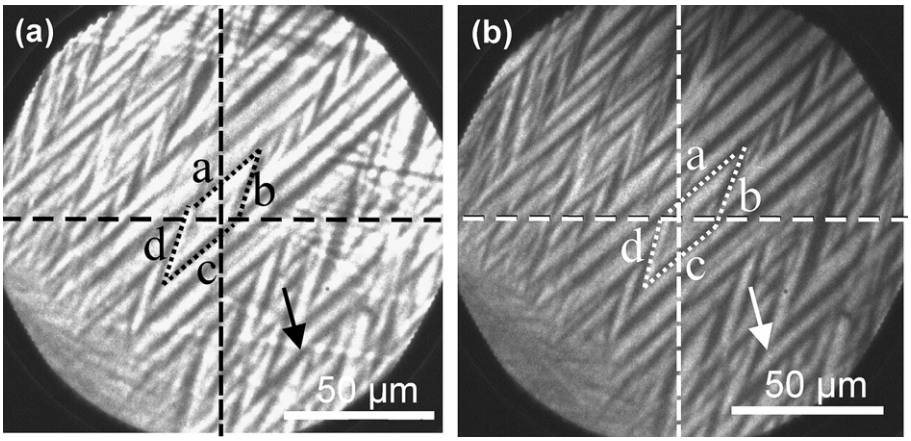

Fig. 5. PEEM images of a CuZnAl surface showing (a) the low-temperature martensite phase and (b) the high-temperature austenite phase in the same area. The position of a polishing scratch, visible on the martensite surface but not on the austenite surface, is marked by the arrow. The diamond marks a set of four, self-accommodated variants that are displaced by the transformation.

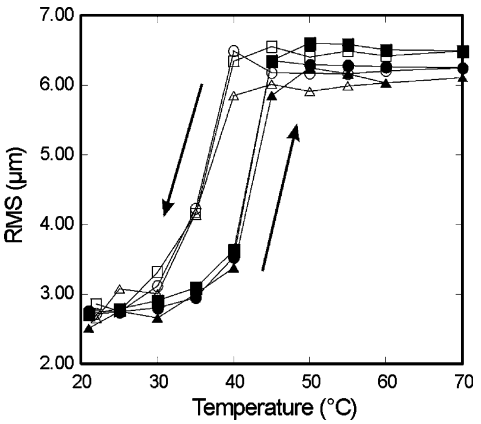

Fig. 6. Root-mean-square roughness of a CuZnAl surface versus temperature during a thermal cycle. Three line profiles are superimposed: solid symbols for heating and open symbols for cooling.

appearance and disappearance of these features are closely related to the martensitic transformation. Wrinkle formation in thin-film SMAs will be addressed in a separate report.

3.2. Photoelectron intensity versus temperature

The martensitic transformations in this work are associated with large changes in PEEM intensity: the PEEM images of the high-temperature phase are darker than the images of the lower temperature phase for both alloys (Figs. 5 and 7). Quantitative measurements of the integrated image intensities during heating and cooling are plotted in Fig. 8. The transition temperatures are readily identified from these plots. For the CuZnAl sample, the PEEM intensity drops sharply at 47 °C during heating and increases sharply at 43 °C during cooling, in agreement with the transition temperatures measured by DSC (Fig. 3). The changes in PEEM intensity are more complicated for the NiTiCu thin film. During heating, the PEEM intensity increases from 30 °C to around 45 °C, remains nearly constant until 70 °C, and then decreases monotonically from 70 to 120 °C. The onset of the monotonic decrease near 70 °C corresponds roughly to the onset of the phase transformation in film stress measurements (Fig. 4). During cooling, the photoelectron intensity increases slowly from 120 °C to 55 °C, then rises rapidly to levels associated with the early stages of heating between 55 and 50 °C.

The rapid rise in photoemission intensity near 55 °C in the NiTiCu thin film contrasts markedly with the more gradual change in film stress during cooling in Fig. 4. We suggest that the martensitic transformation during cooling proceeds gradually through the interior of the film, but that the transformation at the surface is more sudden. This would be the case, for instance, if the transformation to martensite begins at the film–substrate interface and progresses toward the surface. When the interface between the (mostly) martensite and (mostly) austenite phases reaches the surface, a sudden change in photoemission intensities would be observed. Since the photoelectrons originate within nanometers of the surface, PEEM intensities are especially sensitive to conditions along the surface.

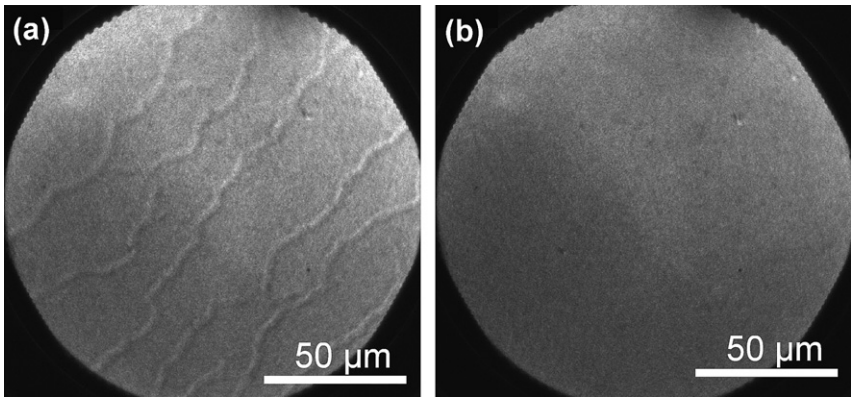

Fig. 7. In situ PEEM images of a NiTiCu thin film at (a) 25 °C (martensite) and (b) 100 °C (austenite).

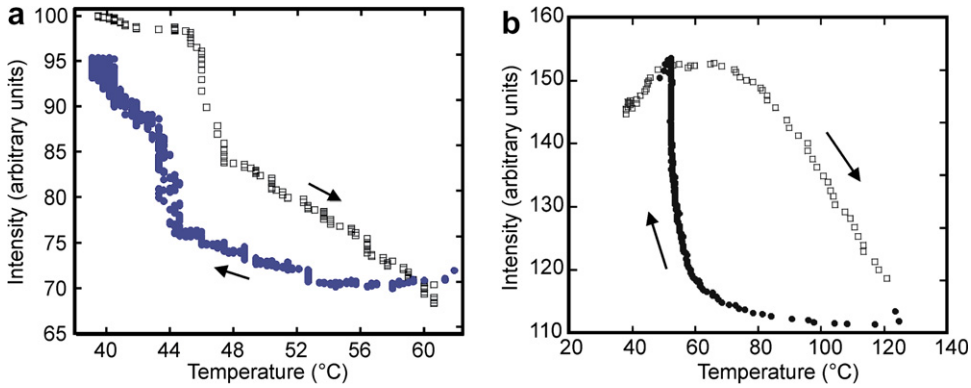

Fig. 8. Integrated PEEM intensities as a function of temperature for (a) CuZnAl and (b) NiTiCu during complete thermal cycles. The arrows indicate the temporal order of data collection.

In general, heating lowers the work function in metals, mainly due to the effect of volumetric expansion. In addition, thermal emission increases exponentially with increasing temperature. Both effects would yield increased emission intensities at higher temperatures. However, the photoemission intensities from the two SMAs are significantly *lower* at the higher temperatures. This is consistent with UPS measurements of apparent work function, shown during complete thermal cycles in Fig. 9. The apparent work function of the CuZnAl SMA increases about 0.23 eV when heated through the transformation temperature, while the apparent work function of the NiTiCu thin film increases about 0.16 eV. Since photoemission intensities depend exponentially on work function, a small increase in work function can significantly reduce the photoemission intensity. We observe virtually no changes in the reflectivity (in the range of 200 nm to 400 nm) between 25 °C to 120 °C, in agreement with Ref. [20]. The observed work function changes can therefore be reasonably attributed to changes in the apparent work function accompanying the solid state phase transformation. The failure of the work function measurements in both materials to return to their initial values during cooling is attributed to localized surface heating by the intense UV source. This results in a temperature difference between the illuminated region and the nearby thermocouple toward the end of the experiment. Work function measurements after cooling overnight agreed well with previous measurements on the room temperature phase.

Although the effect of structure changes on surface work functions is complex, one can account for the lower work function of the martensite phase on the basis of a decrease in the average number of close-packed atomic planes exposed to the surface.

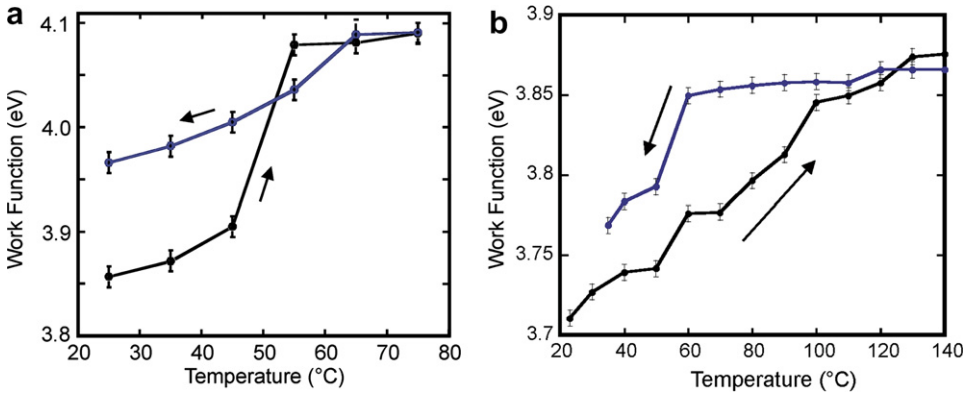

Fig. 9. Apparent work functions determined from UPS data as a function of temperature for (a) CuZnAl and (b) NiTiCu during complete thermal cycles. The arrows indicate the temporal order of data collection.

Wigner and Bardeen's double-layer theory [28,29] relates the lattice structure, interlayer spacing, and the charge distribution to the work function. In particular, more closely packed planes generally have higher work functions (the Smoluchowski effect) [30,31]. Since the austenite to martensite transformation involves a 12% expansion along two axes and a 20% contraction along the third axis, one-third of the planes become somewhat more close-packed and two-thirds become quite a bit less closed-packed. Assuming a random texture distribution in the polycrystalline material, the surface would display all three sets of planes with equal probability. Thus the martensite surface would be dominated by the less close-packed planes. The Smoluchowski effect then leads one to expect the martensite surface to display a lower apparent work function, as observed.

4. Conclusions

Photoemission electron microscopy was used to investigate the thermal-induced phase transformation in two shape memory alloys: polycrystalline CuZnAl and thin-film NiTiCu. UPS measurements of apparent work function during thermal cycling show changes of about 0.23 eV for polycrystalline CuZnAl and about 0.16 eV for thin-film NiTiCu. We attribute the drop in work function and increase in PEEM intensity during cooling to the transformation of surface material from austenite to martensite. The transition temperatures inferred by PEEM are consistent with DSC measurements for CuZnAl and wafer curvature (stress) measurements for thin-film NiTiCu, when account is made for the surface sensitivity of the PEEM technique.

PEEM provides quantitative, spatial resolved information on the evolution of the surface microstructure as the transformation proceeds. Real-time PEEM shows great promise for the quantitative measurement of the kinetics of phase transformations in a wide range of materials and thermal–mechanical processes.

Acknowledgements

This work was supported in part by the Department of Energy Office of Basic Energy Science under Grants DE-FG03-312 02ER45988 and DE-FG03-98ER14864. The PEEM and UPS studies were performed at the W.R. Wiley Environmental Molecular Sciences Laboratory, a national scientific user facility sponsored by the US Department of Energy's Office of Biological and Environmental Research and located at Pacific Northwest National Laboratory. Pacific Northwest National Laboratory is operated for the US Department of Energy by Battelle under Contract DE-AC06-76RLO 1830. The authors thank Dr W.M. Huang, Nanyang Technological University, Singapore, for providing samples and Dr J.J. Zhu, University of Sheffield, for valuable discussions.

References

[1] K. Otsuka, C.M. Wayman (Eds.), Shape Memory Materials, Cambridge University, New York, 1998.
[2] Y.Q. Fu, H.J. Du, W.M. Huang, S. Zhang, M. Hu, Sens. Actuators A 112 (2004) 395.
[3] K. Otsuka, X. Ren, Intermetallics 7 (1991) 511.
[4] Y. Fu, W. Huang, H. Du, X. Huang, J. Tan, X. Gao, Surf. Coat. Technol. 145 (2001) 107.
[5] H. Kahn, M.A. Huff, A.H. Heuer, J. Micromech. Microeng. 8 (1998) 213.

[6] R.H. Wolf, A.H. Heuer, J. Microelectromech. Sys. 4 (1995) 206.
[7] M.J. Wu, W.M. Huang, F. Chollet, Smart Mater. Struct. 15 (2006) N29.
[8] E.C. Bain, N.Y. Dunkirk, Trans. AIME 70 (1924) 25.
[9] K.M. Liew, J.J. Zhu, Mech. Adv. Mater. Struct. 11 (2004) 227.
[10] J.J. Zhu, K.M. Liew, Acta Mater. 51 (2003) 2443.
[11] J.J. Zhu, K.M. Liew, Mech. Adv. Mater. Struct. 11 (2004) 197.
[12] W. Huang, Shape Memory Alloys and their Application to Actuators for Deployable Structures, University of Cambridge, 1998.
[13] Y. Li, L. Cui, Y. Zheng, D. Yang, Mater. Lett. 51 (2001) 73.
[14] W.A. Brantley, M. Iijima, T.H. Grentzer, Thermochim. Acta 392&393 (2002) 329.
[15] J. Antonowicz, A.R. Yavari, G. Vaughan, Nanotechnology 15 (2004) 1038.
[16] S.N. Kulkov, Y.P. Mironov, Nucl. Instrum. and Meth. A 359 (1995) 165.
[17] P. Rittner, P. Lukáš, D. Neov, M.R. Gaymond, V. Novák, G.M. Swallowe, Mater. Sci. Eng. A 324 (2002) 225.
[18] M. Cinchetti, A. Gloskovskii, S. Nepjiko, G. Schonhense, H. Rochholz, M. Kreiter, Phys. Rev. Lett. 95 (2005) 047601.
[19] M.E. Kordesch, in: A.T. Hubbard (Ed.), Encyclopedia of Surface and Colloid Science, Marcel Dekker, New York, 2002, p. 4059.
[20] M. Cai, S.C. Langford, J.T. Dickinson, W.M. Huang, Q. He, T.C. Droubay, D.R. Baer, Proc. ICMEM2005 (2005) 1123.
[21] T.C. Leung, C.L. Kao, W.S. Su, Y.J. Feng, C.T. Chan, Phys. Rev. B 68 (2003) 195408.
[22] W.-C. Yang, B.J. Rodriguez, A. Gruverman, R.J. Nemanich, J. Phys. Condens. Matter 17 (2005) S1415.
[23] G. Ertl, Science 254 (1991) 1750.
[24] G. Xiong, A.G. Joly, W.P. Hess, M. Cai, J.T. Dickinson, J. Chin. Electron Microsc. Soc. 25 (2006) 15.
[25] G. Xiong, A.G. Joly, K.M. Beck, W.P. Hess, M. Cai, S.C. Langford, J.T. Dickinson, Appl. Phys. Lett. 88 (2006) 091910.
[26] W.M. Huang, W.H. Zhang, SPIE Proc. 5277 (2004) 198.
[27] D.Z. Liu, S. Kajiwara, T. Kikuchi, N. Shinya, Phil. Mag. Lett. 80 (2000) 745.
[28] J. Bardeen, Phys. Rev. 49 (1936) 653.
[29] E. Wigner, J. Bardeen, Phys. Rev. 48 (1935) 84.
[30] R. Smoluchowski, Phys. Rev. 60 (1941) 661.
[31] M. Nohlen, M. Schmidt, K. Wandelt, Surf. Sci. 331–333 (1995) 902.